Chemical Engineering Journal 150 (2009) 15–24

Contents lists available at ScienceDirect

Chemical Engineering Journal

journal homepage: www.elsevier.com/locate/cej

Using the Box-Benkhen technique to statistically model phenol photocatalytic degradation by titanium dioxide nanoparticles

Srimanta Ray[a], Jerald A. Lalman[b,*], Nihar Biswas[c]

[a] Department of Civil and Environmental Engineering, University of Windsor, 335 Essex Hall, 401 Sunset Ave., Windsor, Ontario, Canada N9B 3P4
[b] Department of Civil and Environmental Engineering, University of Windsor, 334 Essex Hall, 401 Sunset Ave., Windsor, Ontario, Canada N9B 3P4
[c] Department of Civil and Environmental Engineering, University of Windsor, 136B Essex Hall, 401 Sunset Ave., Windsor, Ontario, Canada N9B 3P4

ARTICLE INFO

Article history:
Received 25 April 2008
Received in revised form
18 November 2008
Accepted 21 November 2008

Keywords:
Photocatalysis
Maximization
Titanium dioxide
Box-Benkhen design

ABSTRACT

A four factor three level Box-Benkhen design (BBD) was developed to describe the photocatalytic degradation of phenol in an aqueous media. The four process variables under consideration in BBD model included titanium dioxide (TiO_2) catalyst size, TiO_2 concentration, dissolved oxygen (DO) concentration and phenol concentration. The model predicted a maximum degradation rate (0.083 min^{-1}) with conditions set at 9.091 nm TiO_2 particle size, 1.0 g/l TiO_2, 31.0 mg/l DO and 40 mg/l phenol. A response outcome computed using experimental data for the 10 nm nanoparticle size catalyst was 13% less than the maximum value. The data suggest that small catalytic particle size augmented the quantum yield in the photocatalytic degradation process with the maximum located at an approximate catalyst size of 10 nm. The photocatalytic degradation rate constant followed an Arrhenius dependency with activation energy of 13.55 kJ/mol K for the 10 nm TiO_2 particles.

1. Introduction

Over the past several decades growing industrial activities have caused an increasing discharge of toxic organic pollutants into the environment. In particular, phenol with an annual global production of approximately 3 million tonnes is one such pollutant [1]. According to Environment Canada's National Pollutant Release Inventory (NPRI) database, approximately 500 tonnes of phenol is discharged annually into the Canadian environment from industries such as petroleum refinery, pulp and paper, metal casting, coal gasification and steel manufacturing [1–5].

Phenol is an endocrine disrupting chemical with carcinogenic, teratogenic, and mutagenic properties [1,3,5–7]. It is used in the manufacture of numerous products for widespread industrial and commercial applications [6]. Phenol and phenol derivatives are present in resins, insulation panels, herbicides and pesticides paints and lubricants [1,3–5,8]. During product manufacturing and wasteland filling, many phenol-based chemicals migrate and make their way into the atmosphere, surface water bodies, groundwater, soils and rocks.

Phenolic-based compounds can be removed from industrial effluents using conventional physical, chemical and biological treatment technologies at varying degree of effectiveness [8–10]. Biological treatment processes are severely impaired beyond threshold levels due to the toxicity caused by phenolics on microorganisms [10,11]. Granular activated carbon (GAC) adsorption has been identified by the United States Environmental Protection Agency (USEPA) as the best available technology (BAT) for treating air and liquid emissions containing phenolic chemicals [12]. Enzymatic treatment methods using tyrosinase, laccase and horseradish peroxidase enzymes have been reported to remove phenols from industrial wastewater [4,10,13,14]. However, because many of the enzymatic processes rely on phase transfer or partial polymerization, phenols and phenol derivatives are not completely removed from the environment.

In recent years, oxidative degradation of organic pollutants in aqueous phase using a photo-illuminated catalyst surface has emerged as a potential technology for treating industrial effluents [15,16]. Heterogeneous photocatalysis offers a unique advantage over other alternative treatment methods because it presents a 'green' treatment approach; since, toxic organic pollutants are converted into carbon dioxide (CO_2) and water using photonic energy [15–17]. Among the reported photocatalysts which have been used, TiO_2 has received the most attention due to its high oxidative potential [17,18]. The oxidative potential of TiO_2 originates from its semiconductor band gap. A photo-illuminated TiO_2 surface generates an electron–hole pair which migrates to the surface of the photocatalyst and initiates the formation of hydroxyl radical ($^{\bullet}OH$). The $^{\bullet}OH$ radicals subsequently mediate the degradation of organic molecules [17–19].

* Corresponding author. Tel.: +1 519 253 3000x2519; fax: +1 519 971 3686.
E-mail address: lalman@uwindsor.ca (J.A. Lalman).

1385-8947/$ – see front matter © 2008 Elsevier B.V. All rights reserved.
doi:10.1016/j.cej.2008.11.039

TiO_2 photocatalysis is affected by the number of photons impinging on the reaction surface and the number of incident photons are an inverse function of the wavelength of incident radiation. Due to the bandgap energy of approximately 3.2 eV, photoexcitation of electrons in TiO_2 is actuated by incident radiation with wavelengths below 380 nm [16,17]. In several batch photocatalytic studies, the UV light irradiance is reported to vary from 4 to 10 mW/cm^2 [17,18,20,21]. The wavelength and irradiance of incident radiation used in many studies are different and this is a major issue preventing the comparison of degradation rates. An alternative approach which can be utilized to compare the rates is to use a parameter known as the quantum yield [18,20,22]. Deriving the quantum yield using data from many studies requires the use of monochromatic light. However, in several studies polychromatic light is used and calculating the quantum yield is not feasible.

Another factor affecting the reaction rate is the surface area per TiO_2 particle. Enhanced TiO_2 photocatalytic efficiency is expected with an increase in the specific surface area of the catalyst or reducing the diffusion path of the charge carrier [23]. TiO_2 particle size within the micrometer range lacks photocatalytic activity because of charge recombination of carriers en-route to the catalyst surface [17,23–25]. Increasing innovations in manufacturing have permitted the production of particle sizes in nanometer range. Several nanometer size TiO_2 formulations have evolved and tested for their photocatalytic potential on selected organic compound such as phenol. Degussa P25 is an exemplary commercially available TiO_2 nanomaterial which has been used to degrade phenol and numerous organic pollutants [18]. Although a few photocatalysis studies have reported using nanometer size TiO_2 catalysts, particle size is not the only parameter which differs between these catalysts [18,22].

Crystal structure is another important catalytic property affecting the degree of photocatalysis. The crystal structure of each forms of TiO_2 is controlled by the semiconductor bandgap. Titanium dioxide exists in four crystalline forms which include anatase (kinetically stable), rutile (thermodynamically stable), brookite and monoclinic-TiO_2. In terms of photocatalytic activity, anatase has the greatest catalytic activity among the various forms. The next structure with less catalytic activity is the rutile form [17,23]. Many photocatalysts including the Degussa P25, which has been utilized for their excellent photocatalytic activity have the anatase crystal structure [18,21,23]. Several studies have reported varying more than one variable (crystal structure and particle size) simultaneously [22,26,27] and hence, comparing the reaction rates for these studies is difficult.

The photocatalytic rate is also affected by the availability of oxygen in the aqueous phase to generate hydroxyl radicals [20,23]. Photocatalysis occurs primarily at the surface and the adsorption properties of the substrate and the quantity of catalytic particles are known to affect the reaction rate [17,19]. Evidence from some studies have shown that adsorption onto the photocatalyst at very low concentrations (less than the 1 mM) follows the Langmuir adsorption isotherm and can be modeled using first-order kinetics [17,20].

Evidence from several reports have described the impact of individual factors on phenolic degradation; however, the photocatalytic rates reported are not comparable due to the difference in reporting units and/or experimental conditions [18,22,23]. Hence, further research is required to consolidate all the factors in a unified model. Accordingly, the effect of TiO_2 particle size (dry), TiO_2 concentration, DO concentration and phenol concentration on the photodegradation rate of phenol will be evaluated using a statistical model.

Using a one-factor-at-a-time optimization approach is a complex method to evaluate the effects of different variables on an experimental outcome. This approach assesses one factor at a time instead of all simultaneously. The method is time-consuming, expensive and often leads to misinterpretation of results when interactions between different components are present. Another approach to accurately evaluate the impact of the variables on the degradation process is to vary all the factors simultaneously in a systematic manner. This approach is referred to as response surface methodology (RSM). RSM is a statistical technique which can address the present scenario under consideration [28–30] and it can be used to establish relationships between several independent variables and one or more dependent variables. Developing a first-degree polynomial model can be performed using statistical experimental designs.

RSM optimizes multiple variables by systematic variation of all variables in a well-designed experiment with a minimum number of experiments. The RSM optimization process involves the following steps: (1) performing statistically designed experiments; (2) estimating the coefficients of a mathematical model using regression analysis technique; and (3) predicting the response and checking the adequacy of the model [28,29]. Among the available statistical design methods, a full factorial design (FFD) is often considered unpractical due to its requirement of a large number of experiments for accurately predicting the response [28,29,31,32]. Fractional factorial design lacks the ability to accurately predict all positions of the factor space that are equi-distant from the centre (rotatability). Based upon the desirable features of othogonality and rotatability, Central Composite design (CCD) and Box-Benkhen design (BBD) are commonly chosen for the purpose of response optimization [29,33].

The BBD technique is a three-level design based upon the combination of two-level factorial designs and incomplete block designs. BBD is a spherical design with excellent predictability within the spherical design space and requires fewer experiments than FFD or CCD with the same number of factors. Compared to the CCD method, the BBD technique is considered as the most suitable for evaluating quadratic response surfaces particularly in cases when prediction of response at the extreme level is not the goal of the model. In addition, the BBD technique is rotatable or nearly rotatable regardless of the number of factors under consideration [28,29,33].

The present study is focused on implementing the BBD technique. Hence, the objective of this study is to optimize the photocatalytic degradation of phenol using a Box-Benkhen experimental design and to develop a predictive model for the phenol degradation rate involving four independent factors. The parameters under investigation are TiO_2 size, TiO_2 concentration, DO concentration and phenol concentration.

2. Materials and methods

2.1. Materials

Titanium dioxide anatase nanoparticles (5, 10 and 32 nm) used in this study were procured from Alfa Aesar (Ward Hill, MA). X-ray diffraction was employed to confirm the anatase crystal structure and the variable under consideration was the particle size (dry). Phenol (Reagent grade (>99% purity)) was purchased from Sigma–Aldrich (Oakville, ON) and ultrapure water (18 MΩ resistivity) was generated using a NANOpure Diamond water unit (Barnstead, IA).

2.2. Photocatalysis of phenol

The photocatalytic experiments were performed in custom-built reaction tubes (25 mm ID × 250 mm length) fabricated from GE-214 clear fused quartz silica (Technical Glass Products Inc., Painesville, OH). Teflon® lined 20 mm septa and aluminum crimp (Cobert Asso-

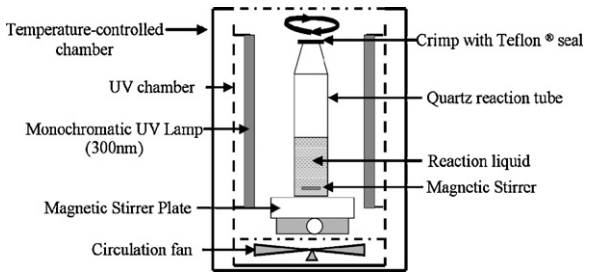

Fig. 1. Schematic diagram of photocatalytic reactor (and experimental apparatus).

ciates, St. Louis, MO) caps were used to seal the reaction tubes. The sealed photocatalytic reaction tubes were placed in a modified Rayonet RPR-100 UV photocatalytic chamber (Southern New England Ultraviolet Co., Branford, CT). The chamber was equipped with sixteen phosphor-coated low-pressure mercury lamps (Southern New England Ultraviolet Co., Branford, CT) on the outer perimeter with a centrally located rotating inner carousel. The inner carousel was set at a constant rotational speed for all the experiments to minimize variation in irradiance between reaction tubes. Three fused quartz reaction tubes triplicates were placed on the inner rotating carousel and the contents were magnetically stirred to maintain the catalyst in suspension, minimize particle agglomeration and also minimize any mass transfer limitation (Fig. 1). The average irradiance emitted from the lamps (300 nm monochromatic UV light) was 9 mW/cm^2. The radiation intensity was measured using a calibrated UV-X radiometer equipped with a 300 nm UV sensor (UV Process Supply, Chicago, IL). The reactor temperature was maintained constant by placing the UV reaction vessel in a temperature controlled chamber. All the photocatalytic experiments, except those performed to evaluate the impact of temperature, were performed at 37 ± 2 °C (310 ± 2 K). The adsorption of phenol onto TiO_2 is not limited near neutral pH and hence, all the experiments were conducted with ultrapure (Milli-Q) water without further pH adjustment [18].

The effects of no oxygen and adding saturated levels of oxygen (BOC Canada, Windsor, ON) on phenol degradation in the presence of TiO_2 was achieved by purging the reaction tube mixture with nitrogen for 1 min (BOC Canada, Windsor, ON) and oxygen, respectively. In the former case, nitrogen was added to the headspace and in the latter, oxygen was added. The tubes were subsequently sealed with 20 mm Teflon® coated silicon rubber septa plus aluminum crimp caps. In experiments conducted with oxygen levels less than that at the saturated level, the headspace was purged and subsequently filled with air (BOC Canada, Windsor, ON). Over the duration of each experiment, a fixed amount of the reaction mixture (1 ml) was withdrawn at specific time intervals and stored in capped tubes wrapped with aluminum foil. After centrifuging the samples, the centrate was analyzed by high performance liquid chromatograph (HPLC). To estimate the quantity of carbon dioxide (CO_2) produced, a fixed amount of headspace gas (50 μl) was withdrawn and analyzed using gas chromatography (GC).

2.3. Analytical measurements and surface area measurements

The phenol concentration was monitored using an HPLC (Dionex Ultimate 3000, Sunnyvale, CA). The instrument was equipped with a UV–visible photodiode array detector set at 215 nm and configured with an Acclaim C18-3 μm—2.1 mm (ID) × 100 mm (length) column (Dionex, Sunnyvale, CA). The analysis was conducted isothermally with the oven temperature set at 45 °C and with an eluent (acetonitrile–water mixture (1:4)) (Fisher Scientific, Ottawa, ON) flow rate set at 0.4 ml/min. The HPLC detection limit for phenol was 5 μg/l.

Headspace CO_2 was analyzed using a Varian CP 3800 GC (Varian, Palo Alto, CA). The GC was configured with a Shin Carbon ST 1 mm (ID) × 2 m (length) column (Restek, Bellefonte, PA) and the hydrogen carrier gas (BOC, Windsor, ON) flow rate was set at 20 ml/min. The analysis was conducted using the following oven temperature program: 80 °C for 0.5 min, ramp to 120 °C at 30 °C/min and hold for 1.0 min then ramp to 150 °C at 40 °C/min. The injection and detector temperatures were set at 100 and 180 °C, respectively. The GC detection limit was 0.2 kPa CO_2.

A dissolved oxygen (DO) probe (YSI 57 DO meter equipped with YSI 5905 DO probe (YSI, Yellow Springs, OH)) was calibrated using known levels of dissolved oxygen. In control studies, the DO levels were monitored for each experimental condition under consideration.

Specific surface area (m^2/g) of the TiO_2 nanoparticles was determined using the Brunauer–Emmett–Teller (BET) gas adsorption technique (Quantachrome NOVA 1200e surface area analyzer, Quantachrome Instruments, Boynton Beach, FL). The instrument temperature was set at 196 °C (77 K) and nitrogen (BOC, Windsor, ON) was the adsorbate.

2.4. Experimental design and statistical analysis

A four factor three level Box-Benkhen design having three central points with three replicates was used to determine the operating conditions for maximizing the phenol degradation rate. The method consisted of defining a minimum or low level (denoted as 1), a central or medium level (denoted as 2) and a high or maximum level (denoted as 3) for each experimental factor (Table 1). The experiments were conducted under the conditions defined in Table 2. A full quadratic model was evaluated for the response function and the experimental data (apparent degradation rate constant (min^{-1})) were analyzed statistically using Minitab 15 (Minitab Inc., State College, PA). Nine experiments (three batches with three replicates) were conducted at the central points to estimate the magnitude of error or "noise" in the experimental analysis. The experiments were performed in a random manner in order to avoid any systematic bias in the outcomes. The responses from process factors other than those selected for the experimental design are considered as error for the experimental design under examination. The coefficients of the quadratic model, which describes the degradation rate (response) as a function of the reaction condition (independent variable), were calculated by a multiple regression analysis on the experimental data. The coefficients were analyzed

Table 1
Four selected factors and three levels.

Levels	Factors			
	TiO_2 nanoparticle size (nm) [specific surface area of TiO_2 nanoparticles (m^2/g)]	TiO_2 catalyst concentration (g/l)	DO concentration (mg/l)	Initial phenol concentration (mg/l)
1	5[a] [275 ± 15 m^2/g][b]	0.1	0.04	40
2	10[a] [131 ± 12 m^2/g][b]	0.5	7.80	70
3	32[a] [47 ± 2 m^2/g][b]	1.0	31.0	100

[a] Particle size.
[b] BET surface area; average and standard deviation for triplicate samples.

Table 2
Design matrix for experimental factors and response at different factor levels.

Expt. order	Factors				Response		
	TiO_2 size (nm)	TiO_2 concentration (g/l)	DO concentration (mg/l)	Phenol concentration (mg/l)	Apparent degradation rate constant (min^{-1})		
					Replicate 1	Replicate 2	Replicate 3
1	10	0.1	0.04	70	0.001	0.0009	0.001
2	10	0.5	7.80	70	0.0127	0.0121	0.0105
3	32	0.5	7.80	40	0.0093	0.0087	0.0093
4	10	0.1	31.0	70	0.0161	0.0165	0.0168
5	10	1	0.04	70	0.0009	0.001	0.001
6	10	0.5	31.0	100	0.0258	0.0235	0.0265
7	10	0.5	7.80	70	0.0068	0.0073	0.0075
8	10	0.5	0.04	100	0.001	0.0007	0.0007
9	32	0.5	7.80	100	0.0036	0.0037	0.0037
10	10	0.5	31.0	40	0.0935	0.0853	0.1053
11	10	0.5	0.04	40	0.0012	0.0013	0.0013
12	5	0.1	7.80	70	0.0069	0.0072	0.0066
13	10	0.1	7.80	100	0.0027	0.0027	0.003
14	5	0.5	31.0	70	0.0231	0.0238	0.0269
15	10	1	7.80	100	0.0036	0.0036	0.0033
16	5	0.5	7.80	40	0.0053	0.0058	0.005
17	32	0.5	0.04	70	0.0002	0.0006	0.0012
18	32	0.5	31.0	70	0.0069	0.0067	0.0075
19	5	0.5	0.04	70	0.0007	0.0008	0.001
20	32	1	7.80	70	0.005	0.0053	0.0059
21	5	0.5	7.80	100	0.0039	0.003	0.0033
22	5	1	7.80	70	0.0041	0.0041	0.004
23	32	0.1	7.80	70	0.0051	0.0049	0.005
24	10	1	7.80	40	0.0074	0.0075	0.0077
25	10	0.5	7.80	70	0.0085	0.0076	0.01
26	10	1	31.0	70	0.0313	0.0402	0.0443
27	10	0.1	7.80	40	0.0056	0.0054	0.0063

using the analysis of variance (ANOVA) to evaluate if a given term has a significant effect ($p \leq 0.05$). The adequacy of the final model was verified by graphical and numerical analysis using the Minitab 15 statistical software [27,31].

The factors and the experimental levels for each factor were selected based on literature values, available resources and results from preliminary experiments. The levels of TiO_2 particle size (dry) were chosen based on the commercial availability of the photocatalyst with the same crystal structure. The maximum and minimum levels of TiO_2 concentrations were determined by preliminary experimental study. Below the lowest TiO_2 concentration, the photocatalytic effect was overwhelmed by photolysis and any further increase in concentration above the highest level was counterproductive due to photo-hindrance caused by the turbidity of the suspension. The maximum and minimum boundaries of the DO concentration were chosen so as to extend the capabilities of the model over the entire range. The phenol concentration was limited by the applicability of the apparent first-order kinetics over the range reported for an industrial effluent [17].

3. Results and discussions

3.1. Phenol photocatalysis

The residual phenol concentration was monitored over a 1-h interval (Fig. 2A) and the disappearance rate (removal) was modeled using equation (1).

$$-\frac{dC}{dt} = kC \tag{1}$$

In Eq. (1), k is the reaction rate constant, referred hereafter as apparent degradation rate constant (min^{-1}), C is the phenol concentration (mg/l) and $(-dC/dt)$ is the first order degradation disappearance (removal) rate. $-\ln(C/C_O)$ was plotted against the reaction time to determine the apparent degradation rate constant (Fig. 2B). Control experiments were performed without the TiO_2

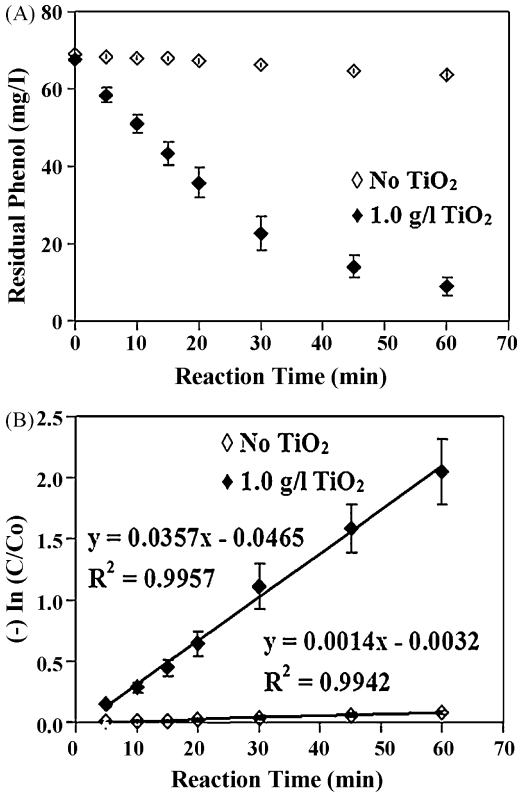

Fig. 2. Phenol degradation profiles for photocatalysis and photolysis. (A) Residual concentration and (B) disappearance (removal) rate. [TiO_2 size: 10 nm; DO concentration: 31.0 mg/l; phenol concentration: 70 mg/l. Average with standard deviation (SD) for triplicate samples is shown.]

catalyst. The quantum yield (ε) was determined using Eq. (2) [20].

$$\varepsilon = \frac{\text{number of phenol molecules degraded per unit time}}{\text{number of incident photon per unit time}} \quad (2)$$

The photolysis quantum yield of approximately 1.5% was significantly lower than the photocatalysis yield of 35%. The higher values observed for the photocatalytic degradation rate and quantum yield were likely due to the higher conversion of photo-generated electrons to hydroxyl radicals on the TiO_2 catalyst surface [17,18].

3.2. Experimental design analysis

For the response surface optimization study, the photocatalytic degradation of phenol was performed at each design point of the four factors (TiO_2 size, TiO_2 concentration, DO concentration and phenol concentration) three levels Box-Benkhen design (Table 1). Considering this design, three sets (replicates) of 27 experiments were performed. The residual phenol concentration was determined at regular intervals over the duration of each experiment and the data were used to compute the apparent degradation rate constant (min^{-1}). The apparent degradation rate constant (k) was considered as the response variable and the computed values at different factor-level combinations were treated statistically to develop the response surface model. The experimental response for the design with the natural level of the experimental factors in form of a matrix is presented in Table 2. A quadratic model described by Eq. (3) was evaluated for the experimental response.

$$\begin{aligned} k = {} & a_0 + a_1 \times (TiO_2 \text{ size}) + a_2 \times (TiO_2 \text{ Conc}) + a_3 \times (\text{DO Conc}) + a_4 \\ & \times (\text{Phenol Conc}) + a_5 \times (TiO_2 \text{ size})^2 + a_6 \times (TiO_2 \text{ Conc})^2 + a_7 \\ & \times (\text{DO Conc})^2 + a_8 \times (\text{Phenol Conc})^2 + a_9 \times (TiO_2 \text{ size}) \\ & \times (TiO_2 \text{ Conc}) + a_{10} \times (TiO_2 \text{ size}) \times (\text{DO Conc}) + a_{11} \times (TiO_2 \text{ size}) \\ & \times (\text{Phenol Conc}) + a_{12} \times (TiO_2 \text{ Conc}) \times (\text{DO Conc}) + a_{13} \\ & \times (TiO_2 \text{ size}) \times (\text{Phenol Conc}) + a_{14} \times (\text{DO Conc}) \times (\text{Phenol Conc}) \end{aligned} \quad (3)$$

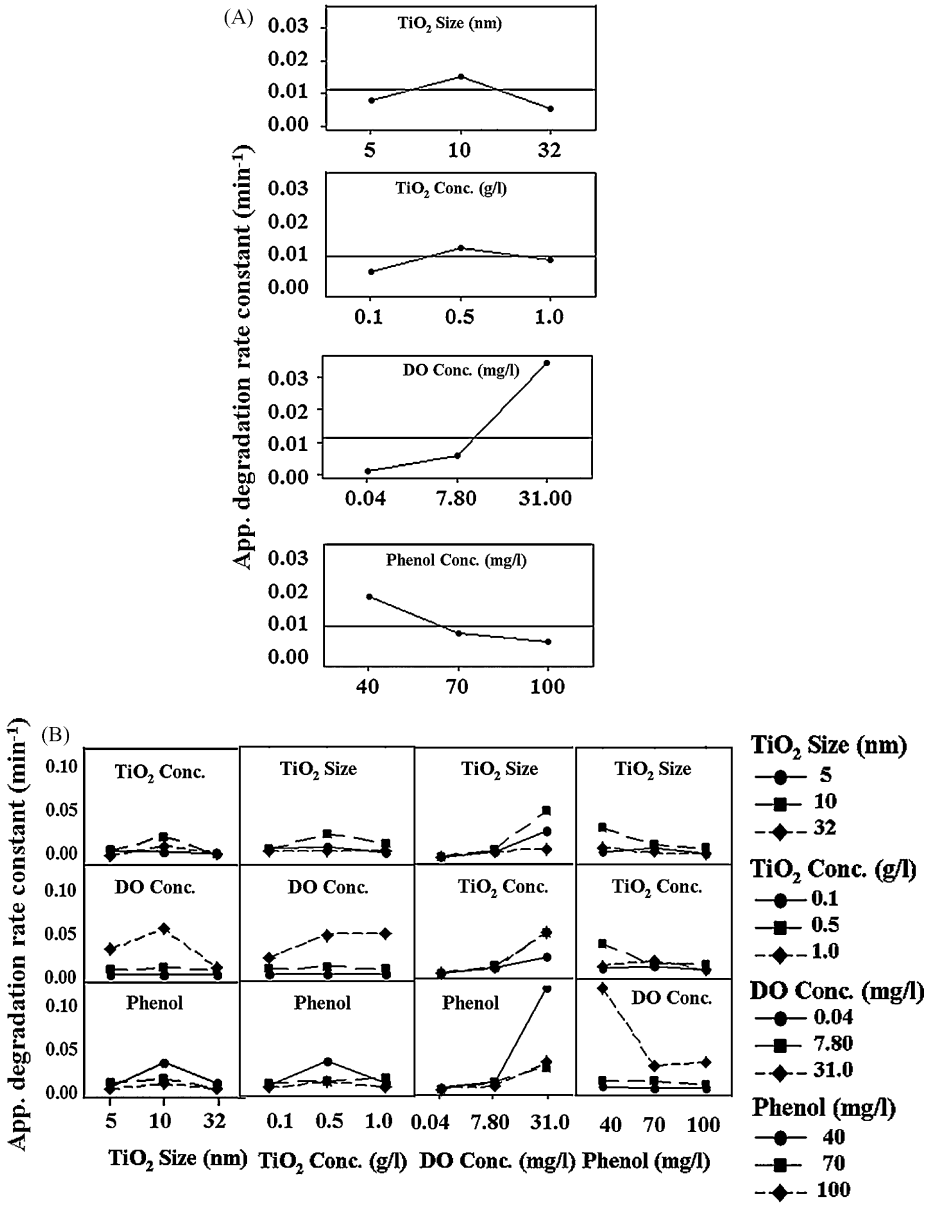

Fig. 3. Matrix of plots of experimental factors for apparent degradation rate constant in a four factors, three levels Box-Benkhen design. (A) Main effects plot and (B) two-factor interaction plots.

3.3. Effects of factors on response variable

The effect of the four factors on the response variable is shown in Fig. 3A. A larger apparent degradation was observed with a TiO_2 particle size set at 10 nm (the middle setting) and a TiO_2 concentration of 0.5 g/l. Notice that greater degradation rates were correlated with higher DO levels. At low phenol levels, the degradation was faster than at higher concentrations. One possible explanation is that at high phenol concentrations competition for active sites of the catalyst is greater than that at the lower concentration. In addition, loss of photons due to absorption by the substrate molecule could also contribute to the lower photocatalytic rate at the higher phenol concentrations. At the lowest DO level (0.04 mg/l), small response values were observed under all the factor-level combinations (Table 2). The largest degradation rate was recorded at 40 mg/l phenol with 0.5 g/l of the 10 nm TiO_2 catalyst and at a DO level of 31.0 mg/l. The higher availability of dissolved oxygen likely enhanced the formation of oxidative radicals and increased the photocatalytic rates. A plot of the two-factor interaction matrix (Fig. 3B) showed evidence of interaction at all factor-level combinations. Contour lines of the response variable (the apparent degradation rate constant (min^{-1})) versus the experimental factors (two-factor-at-a-time) (Fig. 4A–E) connect the points of equal response (equal apparent degradation rate). Strong evidence of interaction between TiO_2 size and DO concentration is shown in Fig. 4A. Notice the contour line trend indicate that high apparent degradation rates are associated with elevated DO levels and lower TiO_2 particles size. Similarly, larger increases were observed for elevated TiO_2 concentrations as the oxygen concentration increased (Fig. 4B). The data presented in Fig. 4B describe the impact of the TiO_2 concentration

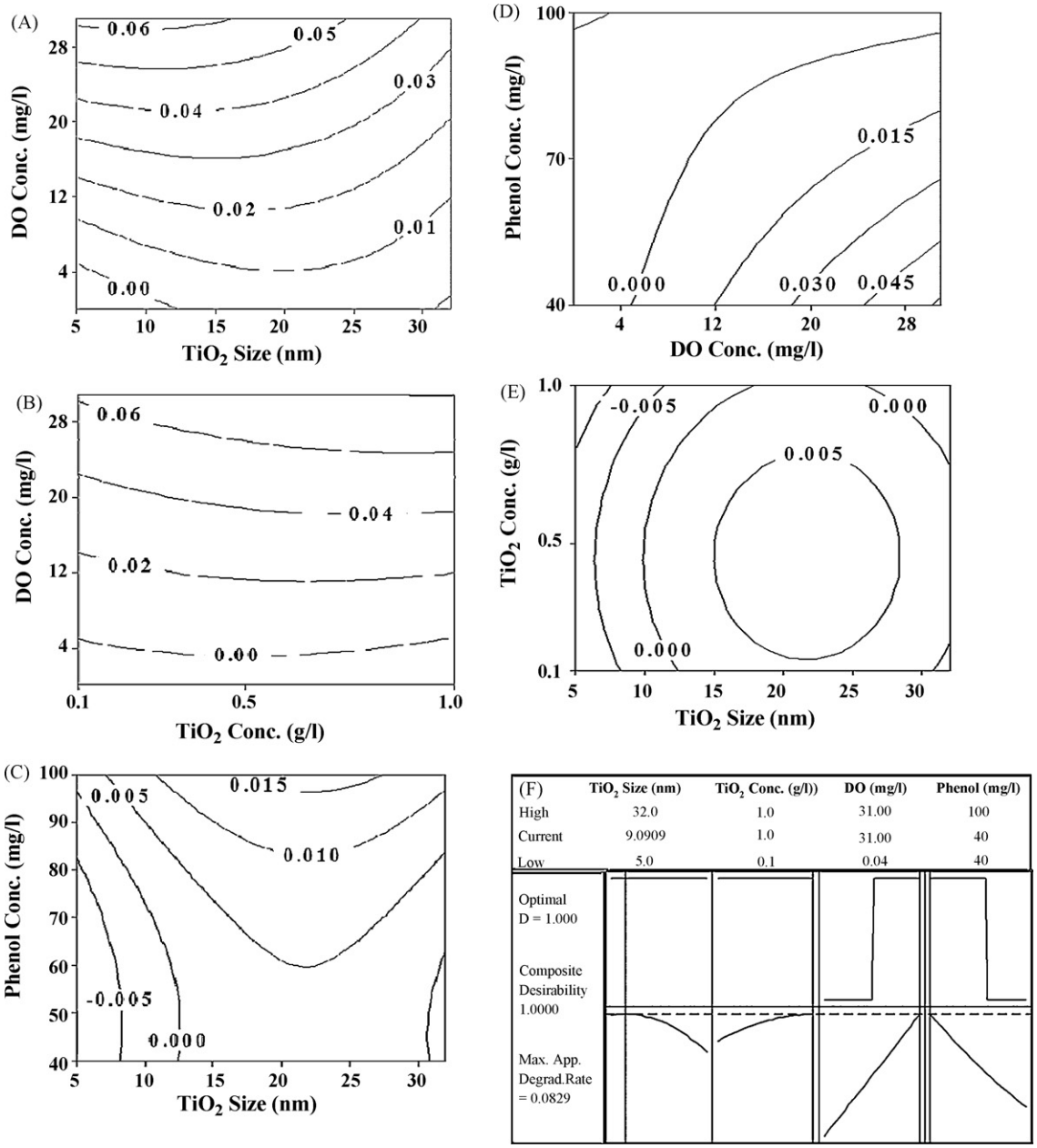

Fig. 4. Effect of design factors on the response variable (apparent degradation rate constant). (A) Contour plot of response for DO concentration and TiO_2 size. (B) Contour plot of response for DO concentration and TiO_2 concentration. (C) Contour plot of response for phenol concentration and TiO_2 size. (D) Contour plot of response for phenol concentration and DO concentration. (E) Contour plot of response for TiO_2 concentration and TiO_2 size. (F) Optimality plot to locate optimum factor levels for maximized response. [Lines in the contour plots connect the points of equal response (equal apparent degradation rate constant, min^{-1}) for a pair of experimental factors studied.]

on the response variable in comparison to that shown in Fig. 3A. In Fig. 4B, interaction between the TiO_2 concentration and DO concentration is shown. The reaction rate constant was greatest at low TiO_2 particle size and high DO levels. The contour plot for TiO_2 size and phenol concentration (Fig. 4C) revealed that the middle level region of the TiO_2 particle size is more effective in degrading high phenol levels. From the contour plot for phenol concentration and DO concentration (Fig. 4D), a strong interaction between the two factors is observed. Notice the apparent degradation rate was augmented with decreasing phenol levels and increasing DO concentrations. The optimum factor levels at which the apparent degradation rate attains a maximum is expected beyond the factor range under consideration. Because the oxygen concentration beyond the saturation level is not used in many treatment systems, additional experiments were not conducted beyond the upper range under examination in this study. The contour plot of the apparent degradation rate for TiO_2 size and TiO_2 concentration predicted a polynomial relation of the response variable (Fig. 4E). A maximum response was expected near the mid-region of the factor space. Further optimization analysis was performed to locate the region of maximum response. The numerical optimization function in the Minitab software, based on the *D*-optimality index, was used to locate the maximum response within the factor-space under evaluation. The *D*-optimality index varied between zero (worst case) and one (ideal case) for all the factors. The software searches for all possible factor settings and computes a value for the largest *D*-optimality value. The optimality plot for the apparent degradation rate, beginning from the low setting for all four factors under consideration, is presented in Fig. 4F. A *D*-optimality of 1.00 with a maximum response (apparent degradation rate) value of 0.083 min^{-1} was recorded at 40 mg/l phenol using a TiO_2 particle size of 9.091 nm together with 1.0 g/l TiO_2 and 31.0 mg/l DO. In comparison, the degradation rate computed using experimental data at 10 nm TiO_2, 1.0 g/l concentration, 31.0 mg/l DO concentration and 40 mg/l phenol concentration was 0.072 min^{-1} (with standard deviation of 0.002 min^{-1}). The experimental response is 13% less than the predicted maximum response. The predicted factor setting of the TiO_2 particle size for a maximum response corresponded with the experimental particle size of 10 nm which was used to develop the model.

3.4. Development of the response surface model

An analysis of variance (ANOVA) was performed to evaluate a full quadratic response surface model presented (Eq. (1)). The ANOVA results (Table 3) of the experimental data reveal that the model is statistically significant with linear, quadratic and interaction terms. Note the differences between replicates are statistically insignificant ($p = 0.816$). A multiple regression analysis was performed on the experimental data to estimate the regression coefficient for the model. The computed regression coefficients for the model along with their respective *p*-values are presented in Table 4. A backward elimination method was applied and statistically insignificant terms ($p > 0.05$) were deleted from the full quadratic model to obtain a final response surface model (Eq. (4)).

Table 3
ANOVA results of the experimental response at different factor levels.

Source	DF[a]	Seq SS[b]	*F*	*p*
Blocks	2	0.000028	0.20	0.816
Regression				
Linear	4	0.014907	14.63	0.000
Square	4	0.001541	5.47	0.001
2-Factor interaction	6	0.007095	17.01	0.000
Residual error				
Lack-of-fit	64	0.004589		
Total	80	0.028132		

[a] DF = degrees of freedom.
[b] Seq SS = sequential sum of square.

Table 4
Response surface model regression coefficients for the apparent degradation rate constant.

Term	Coefficient	Regression coefficient	*p*
Constant	a_0	-0.0117166	0.514
TiO_2 Size	a_1	0.0022244	0.017
TiO_2 Conc.	a_2	0.0200750	0.278
DO Conc.	a_3	0.0037492	0.000
Phenol Conc.	a_4	-0.0004234	0.234
TiO_2 Size×TiO_2 Size	a_5	-0.0000523	0.013
TiO_2 Conc×TiO_2 Conc.	a_6	-0.0224267	0.036
DO Conc.× DO Conc.	a_7	0.0000117	0.341
Phenol Conc×Phenol Conc.	a_8	0.0000044	0.065
TiO_2 Size×TiO_2 Conc.	a_9	0.0000300	0.933
TiO_2 Size× DO Conc.	a_{10}	-0.0000430	0.000
TiO_2 Size×Phenol Conc.	a_{11}	0.0000007	0.890
TiO_2 Conc.× DO Conc.	a_{12}	0.0008159	0.013
TiO_2 Conc.×Phenol Conc.	a_{13}	-0.0000021	0.991
DO Conc.×Phenol Conc.	a_{14}	-0.0000414	0.000

Note: Shaded values are statistically significant at 5% level of significance.

$$k = 0.0022244 \times (TiO_2\ \text{size}) + 0.0037492 \times (\text{DO Conc}) - 0.0000523 \times (TiO_2\ \text{size})^2 - 0.0224267 \times (TiO_2\ \text{Conc})^2 - 0.0000430 \times (TiO_2\ \text{size}) \times (\text{DO Conc}) + 0.0008159 \times (TiO_2\ \text{Conc}) \times (\text{DO Conc}) - 0.0000414 \times (\text{DO Conc}) \times (\text{Phenol Conc}) \quad (4)$$

3.5. Verification of the response surface model

A scatter plot of the experimental data against values predicted by the model (Fig. 5A) revealed a reasonable correlation for all levels (experimental orders). The residuals (difference between the predicted and experimentally apparent degradation rate) are important indicators which are useful in judging the adequacy of fitting the model to experimental data. A normal distribution of residuals ensures an adequate fit of the model with the experimental data. The Anderson–Darling statistic was used to confirm normal distribution of the residuals (Fig. 5B) [34]. The calculated Anderson–Darling (AD) statistics (0.736) was less than the critical value of the statistic (0.752) for a sample size of 81 and at a 5% level of significance [34,35]. A *p*-value of 0.053 (greater than 0.05) confirms a normal distribution of residuals and suggests the model prediction correlated reasonably well with the experimental results over the factor-space analyzed in the study. The results of a two sample *t*-test suggest that the difference between the experimental mean and model predicted mean value of response (apparent degradation rate) is statistically insignificant at a 95% level of confidence. For the two sets of data under consideration, the difference between the mean values is statistically insignificant when $t_{computed}$ (1.45) is less than $t_{tabulated}$ (1.66) [35].

Additional experiments were conducted to confirm the validity and accuracy of the response surface model within the design variables under consideration. A separate validation study was performed for each of the four factors under evaluation and the model prediction was in agreement with the observed results for phenol levels ranging from 40 to 100 mg/l (Fig. 6A). For the DO concentration, the predicted results were consistent with the values observed. However, at high DO levels the model over-estimated the apparent degradation rate (Fig. 6B). Notice the trends for varying TiO_2 concentrations (Fig. 6C) and TiO_2 sizes (Fig. 6D) agreed with

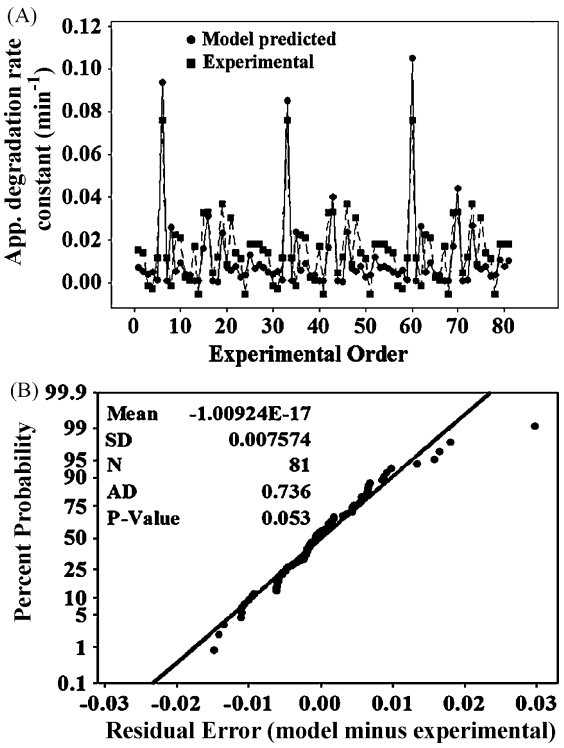

Fig. 5. Assessing the accuracy of the response surface model. (A) Scatter plot of the apparent degradation rate constant against experimental order (81 experiments). (B) Anderson–Darling normality plot of residuals. [AD: Anderson–Darling statistic; *N*: sample size; *p*: level of confidence; Mean: mean value of residual for the apparent degradation rate constant (difference between model prediction and experimental result); SD: standard deviation of the residuals for 81 experiments (*N*).]

the experimental observations. The predicted value was slightly over-estimated compared to the actual observations for low and high TiO_2 concentrations and for the mid and high TiO_2 particle sizes.

3.6. Quantum yield, mineralization rate and temperature dependency of the catalyst

Quantum yields (%) were computed for each of the three TiO_2 particle size. A plot of the quantum yield and specific surface area against particle size suggests that an increase in the specific surface area augmented the quantum yield during the photocatalytic degradation process within the high and mid TiO_2 particle sizes under consideration. As the TiO_2 catalyst particle size was reduced from 10 to 5 nm with a corresponding increase in the specific surface area, the quantum yield did not improve (Fig. 7). A correlation between the model and experimental data for the quantum yield and the specific surface area confirms that the optimum TiO_2 particle size is approximately 10 nm. The lower quantum yield observed below the optimum TiO_2 size could be attributed to the quantum size effect. This effect relates to the confinement of charge carriers (electron or hole) and an increase in bandgap as the particle size approaches the order of de-Broglie wavelength of the charged carrier [19,23].

Experiments were performed at the optimum experimental factor settings for the highest phenol level under consideration. The degradation (or mineralization) rate was estimated by measuring the quantity of CO_2 formed in the headspace. Complete degradation of phenol was evident after 4 h of reaction (Fig. 8A) and the mineralization rate followed zero-order kinetics (Fig. 8B) with a rate constant of 0.0012 mmol CO_2/min.

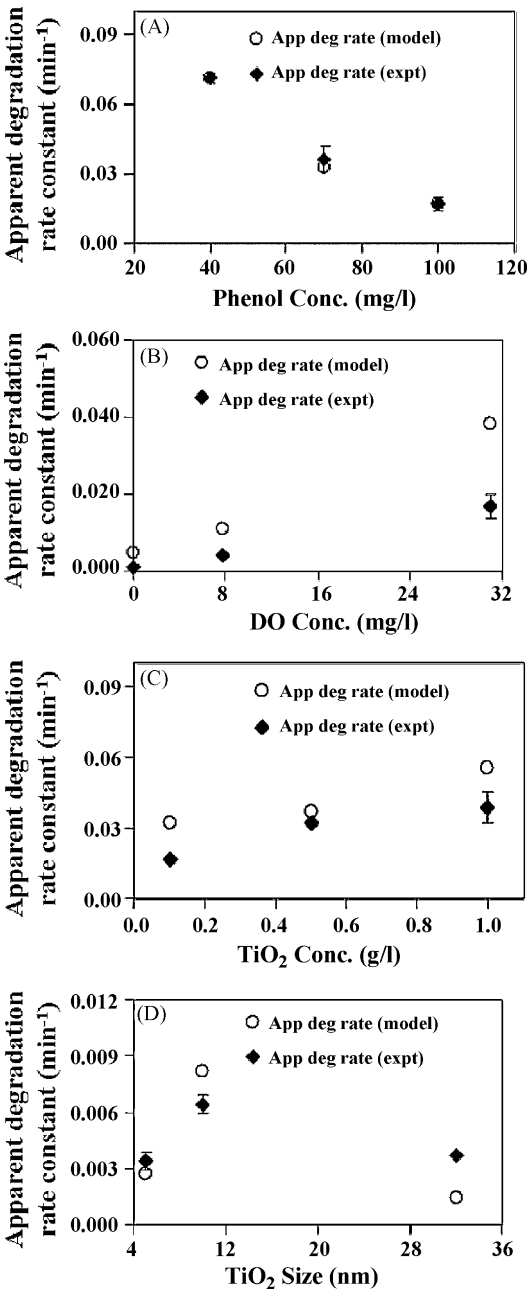

Fig. 6. Validation of the response surface model for the design factors under consideration. (A) Apparent degradation rate constant versus phenol concentration [TiO_2 size: 10 nm; TiO_2 concentration: 1.0 g/l; DO concentration: 31.0 mg/l]. (B) Apparent degradation rate constant versus DO concentration [TiO_2 size: 10 nm; TiO_2 concentration: 1.0 g/l; phenol concentration: 100 mg/l]. (C) Apparent degradation rate constant versus TiO_2 concentration [TiO_2 size: 10 nm; DO concentration: 31.0 mg/l; phenol concentration: 100 mg/l]. (D) Apparent degradation rate constant versus TiO_2 size [TiO_2 concentration: 0.5 g/l; DO concentration: 7.8 mg/l; phenol concentration: 100 mg/l]. [Average with standard deviation (SD) for triplicate samples is shown.]

Photocatalytic degradation experiments conducted with 100 mg/l phenol were performed under 3 temperature conditions (23 °C (300 K), 30 °C (303 K) and 37 °C (310 K)) in the presence of a 10 nm TiO_2 catalyst at a concentration of 1.0 g/l and with a DO level set at 31 mg/l. The photocatalytic degradation rate constant, k_t, (mol s^{-1}) was computed and a plot (Fig. 9) of $-\ln k_t$ versus $1/T$ showed evidence of an Arrhenius dependency of the degradation rate constant. For the 10 nm particle size TiO_2 photocatalyst, the calculated activation energy of 13.55 kJ/mol K is within the range of values reported for the Degussa P25 TiO_2 photocatalyst [36].

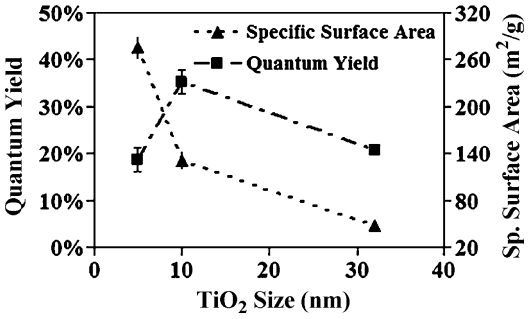

Fig. 7. Quantum yield and specific surface area versus TiO_2 size. [TiO_2 Conc.: 0.5 g/l; DO concentration: 7.8 mg/l; phenol concentration: 100 mg/l. Average with standard deviation (SD) for triplicate samples is shown.]

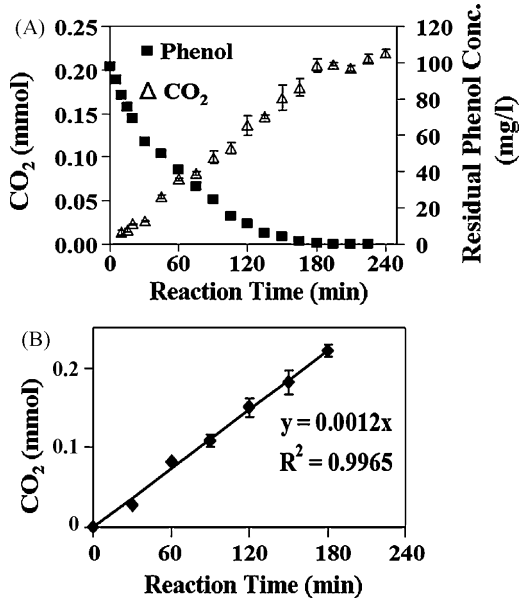

Fig. 8. Mineralization profile for phenol during photocatalysis. (A) Carbon dioxide formation and residual phenol concentration profiles. (B) Mineralization rate profile. [TiO_2 size: 10 nm; TiO_2 concentration: 1.0 g/l; DO concentration: 31.0 mg/l; phenol concentration: 100 mg/l. Average with standard deviation (SD) for triplicate samples is shown.]

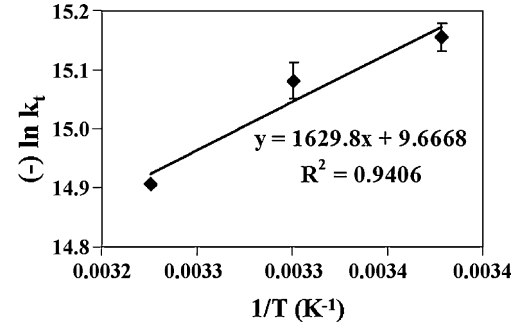

Fig. 9. Arrhenius plot of photocatalytic degradation rate constant for phenol. [TiO_2 size: 10 nm; TiO_2 concentration: 1.0 g/l; DO concentration: 31.0 mg/l; phenol concentration: 100 mg/l. Average with standard deviation (SD) for triplicate samples is shown.]

4. Conclusion

A response surface model, based on the Box-Benkhen technique, was developed to describe the photocatalytic degradation of phenol in an aqueous media. A maximum degradation rate constant of 0.083 min^{-1} was predicted with 40 mg/l phenol concentration, 31 mg/l DO, a TiO_2 particle size of 9.091 nm and 1.0 g/l TiO_2. Using the factor values from the model, the experimental degradation rate of 0.072 min^{-1} was approximately 13% less than the optimum response value for 10 nm nanoparticles.

Increasing the specific surface area by reducing the particle size within the nanometer range enhances the phenol photocatalytic degradation rate. The degradation rate reached a maximum ($0.072 \pm 0.002\ min^{-1}$) with a catalyst particle size of 10 nm. The highest quantum yield ($35 \pm 2.5\%$) was observed for TiO_2 particle size in the range of approximately 10 nm. Other than the catalyst size, the catalyst concentration and DO concentration had a significant impact on the apparent degradation rate. At low phenol levels, the degradation rate constant was greater when compared to elevated phenol concentrations.

The model deviated from the experimental data at high and low settings of the various experimental factors. Hence, further work is in progress to refine the model for improved prediction of the apparent degradation rate constant. The photocatalytic degradation rate constant followed an Arrhenius relationship with an activation energy of 13.55 kJ/mol K for 10 nm TiO_2 particle size.

Acknowledgements

Financial support for this work was provided by the Natural Sciences and Engineering Research (NSERC) of Canada and the University of Windsor.

References

[1] Environmental Health Criteria No. 161, Phenol, http://www.inchem.org/documents/ehc/ehc/ehc161.htm (accessed Feb'08).
[2] http://www.ec.gc.ca/pdb/querysite/results_e.cfm? (accessed Sep'07).
[3] http://www.hc-sc.gc.ca/ewh-semt/alt_formats/hecs-sesc/pdf/pubs/contaminants/psl2-lsp2/phenol/phenol_e.pdf (accessed Sep'07).
[4] J. Wu, K.E. Taylor, J.K. Bewtra, N. Biswas, Optimization of the reaction conditions for enzymatic removal of phenol from wastewater in the presence of polyethylene glycol, Water Res. 27 (1993) 1701–1706.
[5] http://www.osha.gov/SLTC/healthguidelines/phenol/recognition.html (accessed Sep'07).
[6] Y.F. Meknassi, R.D. Tyagi, R.Y. Surampalli, C. Barata, M.C. Riva, Endocrine-disrupting compounds in wastewater, sludge-treatment processes, and receiving waters: overview, Pract. Periodical Haz. Toxic Radioactive Waste Mgmt. 8 (2004) 39–56.
[7] B. Bukowska, S. Kowalska, The presence and toxicity of phenol derivatives—their effect on human erythrocytes, Curr. Top. Biophys. 27 (2003) 47–51.
[8] B.S. Sobecka, M. Tomaszewska, A.W. Morawski, Removal of micropollutants from water by ozonation/biofiltration process, Desalination 182 (2005) 151–157.
[9] P. Westerhoff, Removal of endocrine disruptors, pharmaceuticals and personal care products during water treatment, Southwest Hydrol. 2 (2003) 18–19.
[10] A.B. Martinez, E. Barbot, B. Marrot, P. Moulin, N. Roche, N, Degradation of synthetic phenol containing wastewater by MBR, J. Membr. Sci. 281 (2006) 288–296.
[11] R.L. Autenrieth, J.S. Bonner, A. Akgerman, M. Okaygun, Biodegradation of phenolic wastes, J. Hazard. Mater. 28 (1991) 29–53.
[12] http://www.epa.gov/nrmrl/pubs/625r00015/625r00015.pdf.
[13] S. Kurniawati, J.A. Nicell, Kinetic model of laccase-catalyzed oxidation of aqueous phenol, Biotechnol. Bioeng. 91 (2005) 114–123.
[14] J.V. Bevilaqua, M.C. Cammarota, D.M.G. Freire, G.L. Sant'Anna, Phenol removal through combined biological and enzymatic treatments, Braz. J. Chem. Eng. 19 (2002) 151–158.
[15] D.F. Ollis, E. Pelezzetti, N. Serpone, Photocatalyzed destruction of water contaminants, Environ. Sci. Technol. 25 (1991) 1522–1529.
[16] R.W. Matthews, Photocatalytic oxidation of organic contaminants in water: an aid to environmental preservation, Pure Appl. Chem. 64 (1992) 1285–1290.
[17] J.M. Herrmann, Heterogeneous photocatalysis: state of the art and present applications, Top. Catal. 34 (2005) 49–65.
[18] D.S. Bhatkhande, V.G. Pangarkar, A.A.C.M. Beenackers, Photocatalytic degradation for environmental applications—a review, J. Chem. Technol. Biotechnol. 77 (2001) 102–116.
[19] L. Linsebigler, G. Lu, J.T. Yates Jr., Photocatalysis on TiO_2 surfaces: principles, mechanisms and selected results, Chem. Rev. 95 (1995) 735–758.
[20] S.K. Lee, A. Mills, Detoxification of water by semiconductor photocatalysis, J. Ind. Eng. Chem. 10 (2004) 173–187.
[21] P.R. Gogate, A.B. Pandit, A review of imperative technologies for wastewater treatment. I. Oxidation technologies at ambient conditions, Adv. Environ. Res. 8 (2004) 501–551.

[22] L. Davydov, Photocatalytic degradation of organic contaminants: novel catalysts and processes, Ph.D. Dissertation, University of Cincinnati, 2001, pp. 10–20.
[23] O. Carp, C.L. Huisman, A. Reller, Photoinduced reactivity of titanium dioxide, Prog. Solid State Chem. 32 (2004) 33–177.
[24] D.C. Hurum, A.G. Agrios, S.E. Crist, K.A. Gray, T. Rajh, M.C. Thurnauer, Probing reaction mechanisms in mixed phase TiO_2 by EPR, J. Electron. Spectrosc. Relat. Phenom. 150 (2006) 155–163.
[25] N.S. Allen, M. Edge, A. Ortega, G. Sandoval, C.M. Liauw, J. Verran, J. Stratton, R.B. McIntyre, Degradation and stabilisation of polymers and coatings: nano versus pigmentary titania particles, Polym. Degrad. Stab. 85 (2004) 927–946.
[26] D. Chen, A.K. Ray, Photodegradation kinetics of 4-nitrophenol in TiO_2 suspension, Water Res. 32 (1998) 3223–3234.
[27] A. Salinaro, A.V. Emeline, J. Zhao, H. Hidaka, V.K. Ryabchuk, N. Serpone, Terminology, relative photonic efficiencies and quantum yields in heterogeneous photocatalysis. Part II. Experimental determination of quantum yields, Pure Appl. Chem. 71 (1999) 321–325.
[28] R.H. Myer, D.C. Montogomery, Response Surface Methodology: Process and Product Optimization using Designed Experiment, second ed., John Wiley and Sons, New York, 2002, pp. 343–350.
[29] S. Ray, RSM: a statistical tool for process optimization, Ind. Tex. J 117 (2006) 24–30.
[30] G.E.P. Box, N.R. Draper, Empirical Model Building and Response Surfaces, John Wiley & Sons, New York, 1987, pp. 477.
[31] G.E.P. Box, W.G. Hunter, W.S. Hunter, Statistics for Experimenters: An Introduction to Design, Data Analysis, and Model Building, John Wiley and Sons, New York, 1978, pp. 510–536.
[32] R.H. Myer, A.I. Khuri, W.H. Carter, Response surface methodology: 1966–1988, Technometrics 31 (1989) 137–157.
[33] S. Bae, M. Shoda, Statistical optimization of culture conditions for bacterial cellulose production using Box-Behnken design, Biotechnol. Bioeng. 90 (2005) 20–28.
[34] M.A. Stephens, EDF statistics for goodness of fit and some comparisons, J. Am. Stat. Soc. 69 (1974) 730–737.
[35] D.C. Montogomery, Design and Analysis of Experiments, sixth ed., John Wiley and Sons, New York, 2005, pp. 373–606.
[36] O.E. Kartal, M. Erol, H. Oguz, Photocatalytic destruction of phenol by TiO_2 powders, Chem. Eng. Technol. 24 (2001) 645–649.